

Efficient kinetic method for fluid simulation beyond the Navier-Stokes equation

Raoyang Zhang,^{*} Xiaowen Shan,[†] and Hudong Chen[‡]
Exa Corporation, 3 Burlington Woods Drive, Burlington, MA 01803
(Dated: May 25, 2019)

We present numerical evidence indicating that some essential fluid flows at finite Knudsen number (Kn) can be quantitatively simulated by an extended lattice Boltzmann model. The extension is based on the kinetic theory formulation of the lattice Boltzmann method that includes a third order equilibrium distribution function, a sufficiently accurate Gauss-Hermite quadrature, and a regularization procedure. Results from force-driven Poiseuille flow simulations correctly predict the Knudsen's minimum and the asymptotic behavior of flow flux at large Kn .

PACS numbers: 47.11.+j, 51.10.+y, 47.45.Gx, 47.85.Np

Understanding and simulating fluid flows far from equilibrium pose a long standing challenge to fundamental statistical physics as well as to many other science and engineering disciplines [1, 2]. Due to either rarefaction effects or small geometric scales, such flows are characterized by a finite Knudsen number, defined as the ratio between the particle mean free path, l , and the characteristic length, L , $Kn = l/L$. At sufficient large Knudsen numbers, many of the continuum assumptions breakdown [3]. In particular, the Navier-Stokes equation and the no-slip boundary condition become inadequate.

Since the Boltzmann equation is valid for describing fluid flows at any Kn [4], the conventional approach for constructing extended hydrodynamic equations for higher Kn regimes has been through employing higher order Chapman-Enskog approximations resulting in, *e.g.*, the Burnett and super Burnett equations. However, this approach encounters both theoretical and practical difficulties [5, 6]. Alternatively, attempts have been made to extend the Grad's 13 moment system [7] by including contributions of higher kinetic moments [8]. One major difficulty has been the determination of the boundary condition for these moments because only the lowest few have clear physical meanings. In addition, due to the complexity in the resulting equations, application of this method is so far limited to simple one-dimensional situations. Nevertheless, the moment based formulation offers an valuable insight into the basic fluid physics for high Kn flows.

Over the past two decades, the lattice Boltzmann method (LBM) has developed into an efficient computational fluid dynamic (CFD) tool [9]. Due to its kinetic nature, LBM intrinsically possesses some essential microscopic physics ingredients and is well suited for handling more general boundary conditions. Certain characteristic phenomena in micro-channel flows were predicted in LBM simulations at least qualitatively [10, 11, 12, 13, 14, 15]. In addition, by introducing a “stochastic virtual wall collision” process mimicking effects of free particle streaming in a long straight channel [14], analytically known asymptotic behavior at very large Kn were also produced [14]. Nevertheless, being historically developed only to recover fluid physics at the Navier-Stokes level, the existing LBM schemes used in these studies are not applicable to high Kn flows other than for such extremely limited applications. It is important to develop an LBM method

capable of performing accurate simulations of high Kn flows in general.

Recently, based on the moment expansion formulation [16], a systematic theoretical procedure for extending LBM beyond the Navier-Stokes hydrodynamics was developed [17]. In this work, we present a specific extended LBM model from this procedure containing the next order kinetic moments beyond the Navier-Stokes. A three-dimensional (3D) realization of this LBM model employs a 39-point Gauss-Hermite quadrature with a sixth order isotropy. In addition, a previously reported regularization procedure [18], that is fully consistent with the moment expansion formulation, is also incorporated and extended to the same corresponding order. Simulations performed with the extended LBM have shown to capture certain characteristic features pertaining to finite Kn flows. There is no empirical models used in the new LBM.

It is convenient here to interpret the lattice Boltzmann equation according to the Hermite expansion representation. The single-particle distribution function at a set of particular discrete velocity values, $\{\xi_a : a = 1, \dots, d\}$, are used as the state variables to describe the fluid system. The velocity-space discretization is shown to be equivalent to projecting the distribution function onto a sub-space spanned by the leading N Hermite ortho-normal basis, denoted by \mathbb{H}^N hereafter, provided that ξ_a are the abscissas of a sufficiently accurate Gauss-Hermite quadrature [16, 17]. Adopting the BGK collision model [19], the discrete distribution values, f_a , satisfy the following equation:

$$\frac{\partial f_a}{\partial t} + \xi_a \cdot \nabla f_a = -\frac{1}{\tau} \left[f_a - f_a^{(0)} \right] + F_a, \quad a = 1, \dots, d, \quad (1)$$

where τ a relaxation time, $f_a^{(0)}$ the truncated Hermite expansion of the Maxwell-Boltzmann distribution evaluated at ξ_a , and F_a the contribution of the body force term. The truncation level determines the closeness of the above equation to approximate the original continuum BGK equation. A Chapman-Enskog analysis reveals that the Navier-Stokes equation is recovered when the second order moment terms are retained. As the higher order terms are included, physical effects beyond the Navier-Stokes can be captured systematically [17].

In this work we solve Eq. (1) up to the third order, one order

TABLE I: Degree-7 Gauss-Hermite quadratures on Cartesian grid. Listed are the number of points in the symmetry group, p , abscissas, ξ_a , and the weights w_a . Quadratures are named by the convention $E_{D,n}^d$ where the superscript d and subscripts D and n are respectively the number of abscissas, dimension, and degree of algebraic precision. The subscript FS denotes permutations with full symmetry. Note that since all velocities are normalized with sound speed, the Cartesian grid spacing has a unit velocity of $r = \sqrt{3/2}$.

Quadrature	p	ξ_a	w_a
$E_{3,7}^{39}$	1	(0, 0, 0)	1/12
	6	($r, 0, 0$) _{FS}	1/12
	8	($\pm r, \pm r, \pm r$)	1/27
	6	($2r, 0, 0$) _{FS}	2/135
	12	($2r, 2r, 0$) _{FS}	1/432
	6	($3r, 0, 0$) _{FS}	1/1620
$E_{2,7}^{21}$	1	(0, 0)	91/324
	4	($r, 0$) _{FS}	1/12
	4	($\pm r, \pm r$)	2/27
	4	($2r, 0$) _{FS}	7/360
	4	($\pm 2r, \pm 2r$)	1/432
	4	($3r, 0$) _{FS}	1/1620

higher than the Navier-Stokes hydrodynamics in the conventional LBM models [9]. Here, we also set the temperature to be constant that is sufficient for our present investigation of flows at high Kn but low Mach numbers (Ma). Denoting the local fluid density and velocity by ρ and \mathbf{u} , and defining $u_a = \xi_a \cdot \mathbf{u}$ for brevity, in the dimensionless units in which all velocities are normalized by the sound speed, $f_a^{(0)}$ takes the following simple form:

$$f_a^{(0)} = w_a \rho \left[1 + u_a + \frac{u_a^2 - u^2}{2} + \frac{u_a (u_a^2 - 3u^2)}{6} \right], \quad (2)$$

where $u^2 = \mathbf{u} \cdot \mathbf{u}$, and w_a is the quadrature weight corresponding to the abscissa ξ_a . The last term inside the brackets represents the contribution from the third-order kinetic moments [20] which was shown to be related to the velocity-dependent viscosity [21] but generally neglected in the conventional lattice Boltzmann models.

According to the previous analysis [17], the Gauss-Hermite quadrature employed for solving a third-order truncated system must be accurate with the polynomials up to the sixth order. For ease in implementing LBM model on Cartesian coordinates, we use the 3D Cartesian quadrature $E_{3,7}^{39}$, obtained by directly solving the polynomial orthogonal relation [17]. Its 2D projection gives a quadrature $E_{2,7}^{21}$. The abscissas and weights of both quadratures are provided in Table I. Both LBM models can be verified to admit isotropy for tensors of the form $\sum w_a \xi_a \cdots \xi_a$ up to the sixth order instead of fourth.

With such a Cartesian quadrature, Eq. (1) can be simply discretized in physical space and time, yielding a standard lattice

Boltzmann equation of the form:

$$f_a(\mathbf{x} + \xi_a, t + 1) = f_a(\mathbf{x}, t) - \frac{1}{\tau} \left[f_a(\mathbf{x}, t) - f_a^{(0)} \right] + F_a \quad (3)$$

As usual, the “lattice convention” with unity time increment is used here. An LBM computation is generally carried out in two steps: the streaming step in which f_a at \mathbf{x} is moved to $\mathbf{x} + \xi_a$, and the collision step in which $f_a(\mathbf{x})$ is replaced with right-hand-side of Eq. (3). When viewed as a projection of the continuum BGK equation into \mathbb{H}^N , this process introduces an error due to the fact that f_a generally does not entirely lie within \mathbb{H}^N . When the system is not far from equilibrium, such an error is small and ignorable. On the other hand, this error can be resolved via an application on f_a of a “regularization procedure” of Chen *et al.* previously designed for improvement in stability and isotropy [18]. In terms of the Hermite expansion interpretation, the regularization procedure more concisely described as the following. Explicitly, we split the post-streaming distribution into two parts:

$$f_a = f'_a + f_a^{(0)} \quad (4)$$

where f'_a is the deviation from the truncated Maxwellian, or the *non-equilibrium* component, of the distribution. As $f_a^{(0)}$ already lies entirely in \mathbb{H}^N , the projection only needs to be applied to f'_a . Denoting the projection of f'_a by \hat{f}'_a , and using the orthogonality relation of the Hermite polynomials and the Gauss-Hermite quadrature, \hat{f}'_a is given by the pair of relations:

$$\hat{f}'_a = w_a \sum_{n=0}^N \frac{1}{n!} \mathbf{a}^{(n)} \mathcal{H}^{(n)}(\xi_a), \quad a = 1, \dots, d, \quad (5a)$$

$$\mathbf{a}^{(n)} = \sum_{a=1}^d f'_a \mathcal{H}^{(n)}(\xi_a), \quad n = 0, \dots, N, \quad (5b)$$

where $\mathcal{H}^{(n)}$ is the standard n -th Hermite polynomial [16, 22]:

$$\mathcal{H}^{(0)}(\xi) = 1 \quad (6a)$$

$$\mathcal{H}_i^{(1)}(\xi) = \xi_i \quad (6b)$$

$$\mathcal{H}_{ij}^{(2)}(\xi) = \xi_i \xi_j - \delta_{ij} \quad (6c)$$

$$\mathcal{H}_{ijk}^{(3)}(\xi) = \xi_i \xi_j \xi_k - \xi_i \delta_{jk} - \xi_j \delta_{ik} - \xi_k \delta_{ij} \quad (6d)$$

and $\mathbf{a}^{(n)}$ the corresponding Hermite expansion coefficient, both rank- n tensors. The first two Hermite coefficients vanish due to the conservations of mass and momentum. The second and third order Hermite coefficients are:

$$\mathbf{a}^{(2)} = \sum_{a=1}^d f'_a \xi_a \xi_a, \quad \mathbf{a}^{(3)} = \sum_{a=1}^d f'_a \xi_a \xi_a \xi_a, \quad (7)$$

where $\mathbf{a}^{(2)}$ is traceless due to the conservation of energy.

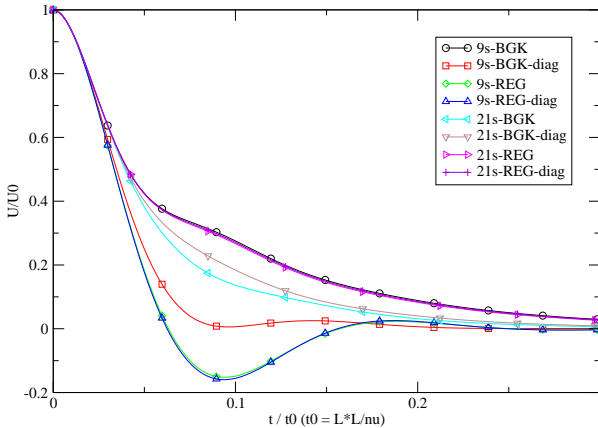


FIG. 1: Peak velocity of a decaying shear waves as simulated by the 9-state (9s) and the 21-state (21s) standard BGK and regularized (REG) models. For each model, simulation is carried out with the wave vector aligned with either the lattice links or their diagonals. The latter is denoted by the post-fix “diag”

Overall, given the discrete non-equilibrium distribution, its projection in \mathbb{H}^3 is fully specified by:

$$\hat{f}'_a = w_a \left[\frac{\mathcal{H}^{(2)}}{2} \sum_{a=1}^d f'_a \xi_a \xi_a + \frac{\mathcal{H}^{(3)}}{6} \sum_{a=1}^d f'_a \xi_a \xi_a \xi_a \right]. \quad (8)$$

With the regularization procedure, Eq. (3) becomes

$$f_a(\mathbf{x} + \boldsymbol{\xi}_a, t + 1) = f_a^{(0)} + \left(1 - \frac{1}{\tau}\right) \hat{f}'_a + F_a. \quad (9)$$

The explicit form of the body force term comes directly from the Hermite expansion of the continuum BGK equation [17, 23]. Up to the third order, it can be expressed as:

$$\begin{aligned} F_a = & w_a \rho \mathbf{g} \cdot (\boldsymbol{\xi}_a + u_a \boldsymbol{\xi}_a - \mathbf{u}) \\ & + \frac{1}{2} w_a \left[\mathbf{a}^{(2)} + \rho \mathbf{u} \mathbf{u} \right] : \left[g_a \mathcal{H}^{(2)}(\boldsymbol{\xi}_a) - 2 \mathbf{g} \boldsymbol{\xi}_a \right]. \end{aligned} \quad (10)$$

To be noted here is that, whereas the first term is entirely due to the equilibrium part of the distribution, the term related to $\mathbf{a}^{(2)}$ are contributions from the non-equilibrium part. To our knowledge, the non-equilibrium contribution in the body-force has not been explicitly considered in the existing LBM literature. Although it is expected to play an important role at large Kn , at moderate Kn (≤ 1), no significant effects due to non-equilibrium contribution are found in the numerical experiments in the present work.

The first series of numerical simulations performed are for the benchmark problem of 2D sinusoidal shear wave decay.

The decay rate of the peak velocity magnitude is measured in two sets of simulations. In the first set, a sinusoidal wave with a wavelength (L) of 128 grid spacing is simulated on a 128×128 periodic domain. The initial velocity field is given by $u_x = u_0 \sin(y/2\pi L)$ and $u_y = 0$. The wave vector is aligned with the lattice. In the second set, the same sinusoidal wave is rotated by 45 degrees and simulated on a matching periodic domain size of $181 (= 128\sqrt{2}) \times 181$. The Knudsen number, defined as $Kn = 2\tau c_s/L$, is chosen to be 0.2, where τ is the relaxation time and c_s the sound speed. The purpose of these tests is to detect any lattice orientation dependent artifacts which often plague discrete fluid models especially when non-equilibrium effects are significant. The two sets of simulations were conducted using four representative models: the popular 2D 9-state (9-s) model (D3Q9), and the new 2D 21-state (21-s) model based on $E_{2,7}^{21}$, both with and without the regularization process. In discussions hereafter we shall refer the models without the regularization as the BGK models, and the ones with regularization the REG models.

In Fig. 1, the dimensionless peak velocity magnitude, normalized by its initial value and measured at the $1/4$ width of wavelength, is plotted against the non-dimensionalized time normalized by the characteristic decay time $t_0 = \lambda^2/\nu$, where $\nu = c_s^2(\tau - 1/2)$ is kinematic viscosity. As expected, the decay rate of the shear wave for the 9-s BGK model is strongly dependent on the orientation of the wave vector with respect to the lattice, indicating a strong anisotropy of the model at this Kn . Interestingly this anisotropy is essentially eliminated by the regularization procedure in the resulting 9-s REG model. However, the amplitude of the shear wave exhibits a strong oscillatory behavior in addition to the exponential decay, implying a greater than physical ballistic effect. These may be explained as the following: The non-equilibrium part of the post-streaming distribution contains contributions from *in principle* all moments, which are highly anisotropic due to inadequate symmetry in the underlying discrete model to allow isotropy beyond the second order. The regularization procedure filters out the higher than the second order moment contributions, yielding an isotropic behavior. On the other hand, the higher moments are critical at large Kn . Clearly, with and without the regularization, the 9-s models do not show satisfactory results at high Knudsen numbers. For the 21-s BGK model, an anisotropic behavior is also very visible, though at a much smaller extent. This may be attributed to the residual anisotropy in the moments higher than the third order. Again, the anisotropy behavior is removed once the regularization procedure is applied. It is also notable that the decay history shows a much reduced oscillatory behavior in the 21-s REG model. It is also curious to observe that the decay of the “lattice aligned” result from 9s-BGK is surprisingly close to that of 21-s REG model at this Kn .

Using the same four models, we subsequently carried out simulations of the force-driven Poiseuille flow for a range of Knudsen numbers. In these, a periodic boundary condition is used in the stream-wise (x) direction, and a standard half-way bounce-back boundary condition is used in the cross-channel

(y) direction. Four grid points are used in the x direction. In the y direction, two different resolutions, $L = 40$ and 80 are tried to ensure sufficient resolution independence. The Knudsen number is defined as $Kn = \nu/(c_s L)$. The flow is driven by a constant gravity force, g , pointing in the positive x direction. The magnitude of the force is set to $8\nu U_0/L^2$, which would give rise to a parabolic velocity profile with a peak velocity of U_0 in the vanishing Kn limit. For consistency, a modified definition of fluid velocity, $\mathbf{u} \rightarrow \mathbf{u} + \mathbf{g}/2$, is used in $f_a^{(0)}$. To enforce an incompressible behavior throughout the simulated Kn range, we choose a sufficiently small value of U_0 , corresponding to the nominal Mach numbers of $Ma (= U_0/c_s) \sim 1.46 \times 10^{-6}$ and 2.92×10^{-7} , and verified that our results are independent of Ma . The actual resulting fluid velocity in these simulations can be values much higher than U_0 at higher Kn .

Plotted in Fig. 2 is the non-dimensionalized mass flux, $Q \equiv \sum_{y=0}^L u_x(y)/Q_0$, as a function of Kn in the final steady state of the simulations. Here $Q_0 = gL^2/c_s$. For comparison we also include two analytical asymptotic solutions [4] for both small and very large Kn . To be noted first is that at the vanishing Kn limit, all simulation results agree with each other as well as with the analytical solution. Also plotted is the exact Navier-Stokes solution of $Q = 1/(12Kn)$. At higher Kn , the 9-s BGK model captures the Knudsen's minimum while overestimates the flux as previously reported [14]. However, by filtering out moment contributions higher than the second order, these phenomena completely disappear from the result of 9-s REG, yielding a purely monotonically decreasing behavior. The results from both the 21-s BGK and the 21-s REG models predict a Knudsen minimum which resemble that of the 9-s BGK except with reduced over-estimation at higher Kn . What is mostly interesting is that the flux behavior predicted by the 21-s REG exhibits a reversal of curvature at higher Kn , consistent with the analytical solution. The qualitatively differences seen from these four models suggest that contributions from moments beyond second order are essential for capturing fundamental physical effects at high- Kn . Although the high-order moments are implicitly contained in the second-order BGK model, its dynamics is highly lattice orientation dependent. In contrary, by incorporating the high-order moments explicitly and systematically, flow at these Kn values can indeed be captured in the extended LBM model.

In summary, kinetic based representation offer a well-posed numerical approach in CFD for simulations of flows at finite Kn . In this work we present a specific extended LBM model that incorporates the effects of high-order kinetic moments. It is robust and highly efficient, and demonstrates a capability in quantitatively capturing certain fundamental flow features at finite Knudsen numbers without introducing empirical modeling. It is also clear that the new LBM model is not limited to specific uni-directional channel flows involving only lattice aligned orientations. Nevertheless, a number of issues are awaiting further studies. For even higher Kn (100), one should expect and straightforward to include moment contri-

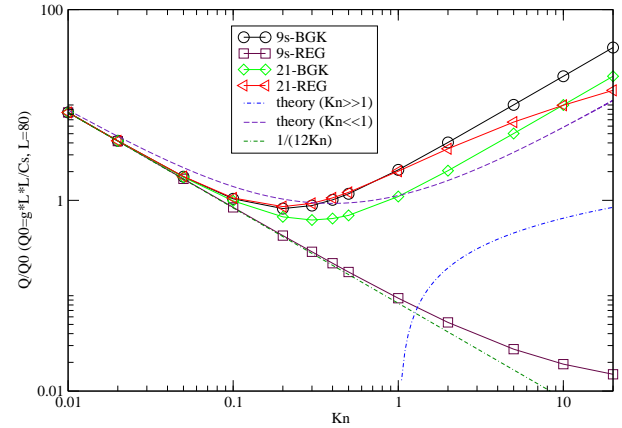


FIG. 2: This figure shows the Knudsen paradox with resolution 40, $Ma = 1.46 \times 10^{-6}$. The Kn which has the minimum Q is about 0.2 for 21s-REG, 0.3 for 21s-BGK and 0.2 for 9s-BGK. The theoretical results are that of Cercignani [4].

butions higher than the third order via the systematic procedure [17]. The issue of boundary condition and thermal effect are also of eminent importance [24, 25, 26], even though the realization of the essential slip-velocity effect and the asymptotic behavior is demonstrated to be attributed to a significant extent to the third order and higher moment contributions in the intrinsic LBM dynamic system itself. As reported in some previous works [13, 14], the kinetic boundary condition of Ansumali and Karlin [27] has lead to substantial improvements at the Navier-Stokes level micro-channel flow simulations. Thermodynamic effect can also be incorporated, as it is expected to become non-negligible at finite Mach numbers. The present third-order model is thermodynamically consistent at the Navier-Stokes level [17]. Another interesting point to mention is that both the 21-s BGK or the 21-s REG can allow an expanded equilibrium distribution form including terms up to the fourth power in fluid velocity (as opposed to the square power in 9-s BGK), for that the correct equilibrium energy flux tensor is still preserved. Including the forth power terms immediately results in a desirable positive-definite distribution for the zero-velocity state at all Mach number values.

* Electronic address: rao.yang@exa.com

† Electronic address: xiaowen@exa.com

‡ Electronic address: hudong@exa.com

[1] J. M. Reese, M. A. Gallis, and D. A. Lockerby, Phil. Trans. Roy. Soc. London A **361**, 2967 (2003).

- [2] C.-M. Ho and Y.-C. Tai, *Annu. Rev. Fluid Mech.* **30**, 579 (1998).
- [3] M. Gad-el-Hak, *J. Fluids Eng.* **121**, 5 (1999).
- [4] C. Cercignani, *Theory and Application of the Boltzmann Equation* (Scottish Academic Press Ltd., New York, 1974).
- [5] R. K. Standish, *Phys. Rev. E* **60**, 5175 (1999).
- [6] R. K. Agarwal, K.-Y. Yun, and R. Balakrishnan, *Phys. Fluids* **13**, 3061 (2001).
- [7] H. Grad, *Commun. Pure Appl. Math.* **2**, 331 (1949).
- [8] H. Struchtrup, *Phys. Rev. E* **65**, 041204 (2002).
- [9] S. Chen and G. Doolen, *Ann. Rev. Fluid Mech.* **30**, 329 (1998).
- [10] X. Nie, G. D. Doolen, and S. Chen, *J. Stat. Phys.* **107**, 279 (2002).
- [11] C. Y. Lim, C. Shu, X. D. Niu, and Y. T. Chew, *Phys. Fluids* **14**, 2299 (2002).
- [12] B. Li and D. Y. Kwok, *Phys. Rev. Lett.* **90**, 124502 (2003).
- [13] X. D. Niu, C. Shu, and Y. T. Chew, *Europhys. Lett.* **67**, 600 (2004).
- [14] F. Toschi and S. Succi, *Europhys. Lett.* **69**, 549 (2005).
- [15] Y. Zhou, R. Zhang, I. Staroselsky, H. Chen, W. Kim, and M. S. Jhon, *Physica A* **362**, 68 (2006).
- [16] X. Shan and X. He, *Phys. Rev. Lett.* **80**, 65 (1998).
- [17] X. Shan, X.-F. Yuan, and H. Chen, *J. Fluid Mech.* **550**, 413 (2006).
- [18] H. Chen, R. Zhang, I. Staroselsky, and M. Jhon, *Physica A* **362**, 125 (2006).
- [19] P. L. Bhatnagar, E. P. Gross, and M. Krook, *Phys. Rev.* **94**, 511 (1954).
- [20] H. Chen, C. Teixeira, and K. Molvig, *Intl. J. Mod. Phys. C* **8**, 675 (1997).
- [21] Y.-H. Qian and Y. Zhou, *Europhys. Lett.* **42**, 359 (1998).
- [22] H. Grad, *Commun. Pure Appl. Math.* **2**, 325 (1949).
- [23] N. S. Martys, X. Shan, and H. Chen, *Phys. Rev. E* **58**, 6855 (1998).
- [24] I. Ginzburg and P. M. Adler, *J. Phys. II France* **4**, 191 (1994).
- [25] I. Ginzburg and D. d'Humières, *J. Stat. Phys.* **84**, 927 (1995).
- [26] H. Chen, C. Teixeira, and K. Molvig, *Intl. J. Mod. Phys. C* **9**, 1281 (1998).
- [27] S. Ansumali and I. V. Karlin, *Phys. Rev. E* **66**, 026311 (2002).